Journal of
Water & Climate Change

IWA PUBLISHING

Journal of Water and Climate Change Vol 14 No 7, 2133 doi: 10.2166/wcc.2023.456

Assessment of impact of climate change on the streamflow of Idamalayar River Basin, Kerala

C. Reshma * and R. Arunkumar

Department of Civil Engineering, National Institute of Technology Calicut, Kozhikode 673601, Kerala
*Corresponding author. E-mail: reshmanarayananc@gmail.com

CR, 0000-0001-7258-0436; RA, 0000-0002-4211-7480

ABSTRACT

This study investigates the impacts of climate change on water availability in the Idamalayar basin, Kerala. Soil and Water Assessment Tool (SWAT), Hydrologic Engineering Centre – Hydrologic Modelling System (HEC-HMS), and bias-corrected climate change data were used to simulate future streamflows. The performances of SWAT and HEC-HMS were assessed using four statistical indices (R^2, Nash–Sutcliffe efficiency, percentage bias, and RSR). SWAT slightly outperformed HEC-HMS. The CMIP6 general circulation models (GCMs) were selected using PROMETHEE-2. The variations in climate variables and streamflows were studied for three future periods, i.e., near-future (2031–2040), mid-future (2051–2060), and far-future (2071–2080) under three shared socio-economic pathway (SSP) scenarios (SSP126, SSP245, and SSP585). The projections of GCMs show different patterns in variation of precipitation. Generally, there is a slight increase in annual precipitation. However, there was a notable decline in peak in July. An additional peak was often seen in October. The maximum and minimum temperatures showed a decreasing trend. The average annual streamflow reduction under SSP126 was approximately 25.63, 27.92, and 26.24% in the near, mid, and far future, respectively. Under SSP245, the average decrease was 30.71, 16.06, and 19.06% for the near, mid and far future, respectively. For SSP585, there was 12.73% increase in the far-future period.

Key words: climate change, general circulation models, HEC-HMS, Idamalayar, streamflow, SWAT

HIGHLIGHTS

- Water availability in the Idamalayar catchment is studied using five CMIP6 GCMs under three SSP scenarios, for three future periods.
- Different GCMs project the variation in water availability differently.
- Generally, there is a decrease in the streamflow except in the far-future period under SSP585.
- The variation in streamflow calls for better management practices.

GRAPHICAL ABSTRACT

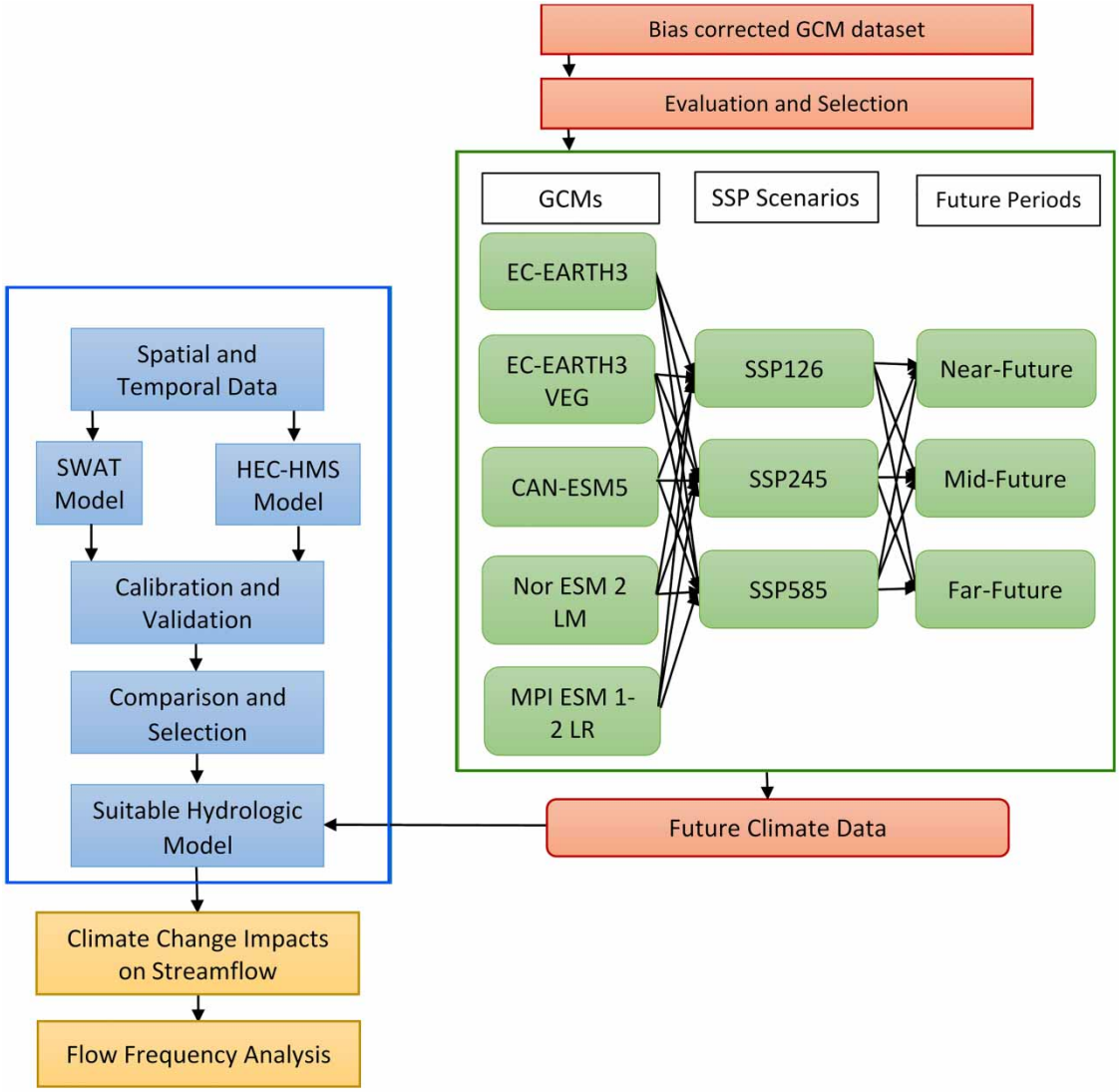

1. INTRODUCTION

The availability of freshwater remains one of the essential perquisites of human existence on the planet. The diminishing quantity and quality of freshwater and its high sensitivity to climate change call for effective and sustainable utilization of this resource in the present and the future (Mandal & Simonovic 2017). Therefore, it is essential for water resources managers and decision-makers to take climate change into account. Several studies have investigated the impact of climate change on water availability in different parts of the world. The general approach to investigate the effect of climate change on the hydrological regime is to simulate the hydrological response of the catchments using a hydrological model utilizing the climatic variables projected by general circulation models (GCMs) (Zhang *et al.* 2016).

Hydrologic models are generally classified into lumped, semi-distributed, and distributed models. Soil and Water Assessment Tool (SWAT) and Hydrologic Engineering Centre – Hydrologic Modeling System (HEC-HMS) are the two semi-distributed hydrological models that are widely used to simulate the responses of a basin. SWAT has been extensively used in modelling streamflow, water quality, and sediment yield. This model has been successfully configured for different river basins across the globe. It has been identified as a valuable and popular tool for environmental and climate change studies. Yaduvanshi *et al.* (2018) used SWAT to model the streamflow under extreme rainfall events. They found that it

performed well in simulating hydrologic responses under extreme events. The SWAT model has also been used in studies investigating the impact of land-use change and climate change on streamflow. For instance, Bhatta *et al.* (2019) examined the effect of climate change on a Himalayan river basin using SWAT. They compared the impact of the complexity of the model on the results based on the number of sub-basins, hydrologic response units (HRUs), and elevation bands. They successfully configured SWAT for the river basin and concluded that including different elevation bands improved the simulation results. In a similar study by Sharma *et al.* (2022), the SWAT model was used for modelling the impacts of land-use and climate changes on the water availability of the Dharoi River basin, India. They compared the model's performance based on different calibration approaches and concluded that the SWAT model was satisfactory in simulating monthly streamflow.

HEC-HMS is another semi-distributed hydrological model widely used for event-based as well as continuous simulations. Oleyiblo & Li (2010) have used the HEC-HMS model for Misai and Wan'an catchments in China to study its applicability in flood forecasting. The results showed that HEC-HMS is suitable for the selected catchments, with a satisfactory prediction of the time of occurrence and volume of flood events. Wijayarathne & Coulibaly (2020) used the HEC-HMS model along with other hydrologic models for the Waterford River watershed, Canada, to study its applicability in streamflow simulation and flood forecasting. They concluded that the model reasonably simulates the streamflow and recommends it for operational use in predicting floods. Palacios-Cabrera *et al.* (2022) used the HEC-HMS model to study the hydrodynamic response of a semi-arid Mediterranean karstic watershed based on land-use change and precipitation cycles. They reported that HEC-HMS gave satisfactory values for the performance indices considered. In general, both the SWAT and HEC-HMS models have been successfully applied to different watersheds and are suitable for streamflow simulation.

In addition to hydrological models, downscaled and bias-corrected GCM outputs are also required for assessing the impact of climate change. The GCMs developed in the sixth phase of Coupled Model Inter Comparison Project (CMIP6) of the Intergovernmental Panel on Climate Change (IPCC) are the most advanced tools for projecting future climate. The CMIP6 projections are available under different shared socio-economic pathway (SSP) scenarios.

By using GCMs, studies have been conducted worldwide to examine the impact of climate change on water resources. In a study by Zhang *et al.* (2016), the hydrologic responses of the Heihe River basin in China were investigated for future climate change scenarios using SWAT and the statistically downscaled climate change data. They found that warmer and wetter trends will be continued in the future. In a similar study by Luo *et al.* (2019), the impact of climate change in nine high-alpine catchments across Xinjiang, China, under two representative concentration pathway (RCP) scenarios, RCP 4.5 and RCP 8.5, was investigated using the SWAT model. It was reported that the future water resource changes in Xinjiang are not sustainable and will lead to a decrease in discharge. Gao *et al.* (2021) studied the impact of climate change on the future streamflow of the Laixi River basin, China, using statistically downscaled CMIP5 GCM outputs and SWAT model under three RCP scenarios (RCP 2.6, RCP 4.5, and RCP 8.5). The streamflow was projected to rise gradually during future periods (i.e., 2050s and 2080s) under all three scenarios. By using bias-corrected Regional Climate Models (RCM) outputs and the Hydrologinska Brans Vattenbalansavdelning (HBV) hydrological model, Abdulahi *et al.* (2022) investigated the effects of climate change on streamflow in the Upper Awash River basin, Ethiopia, under the RCP 4.5 and RCP 8.5 scenarios. The findings indicated that streamflow would rise under both RCPs following the precipitation increment.

Similar studies have been conducted in the Indian subcontinent also. Mudbhatkal *et al.* (2017) assessed the possible impact of climate change on the hydrology of the Malaprabha and Netravati River watersheds in India. They reported that the effect of climate change is evident, but each river responds differently to climate change. In a study by Kumar *et al.* (2017) on the impact of climate change on different water balance components in the upper Kharun catchment, it is reported that the flow will decrease in the 2020s and increase in 2050s and 2080s. Bisht *et al.* (2020) assessed the impact of climate change on the streamflow characteristics of the Mahanadi basin. The mean monthly flow was found to be increasing in the far-future (FF) period (to the end of the century). Jaiswal *et al.* (2020) have conducted a similar study to analyse the impact of climate change on the command area of Tandula dam, India. They found that there would be a decrease in the reservoir water supply due to reduced rainfall. In a similar study by Sadhwani *et al.* (2023), the impact of climate and land-use changes in the Periyar River Basin, Kerala, was investigated using a SWAT model. They pointed out that there are possibilities of reduction in average annual streamflow.

The results of all these studies substantiate the necessity of regional-scale research on climate change impacts on hydrological regimes. For instance, Kerala has witnessed severe floods in the monsoon for two consecutive years, in 2018 and 2019. In the 2018 flood, all 14 districts in Kerala were affected (Pramanick *et al.* 2022). The heavy rainfall and the associated change in discharge complicated reservoir operation. Localized intense rainfall in the upstream and subsequent releases from

reservoirs caused flooding in the downstream (Pramanick *et al.* 2022). The study by Hunt & Menon (2020) has linked the 2018 flood to climate change. It was reported that the future climate would possibly exacerbate the chances of flooding. Sudheer *et al.* (2019), in a study of the role of dams in flooding in the Periyar River Basin, Kerala, concluded that the operating rules of the reservoirs should be revisited to mitigate floods while serving the purposes for which they were designed. For this, knowledge of the future streamflow is required. Idamalayar dam is among the major dams in the Periyar River Basin, with a live storage capacity of 1018 MCM. Also, the Idamalayar catchment received the highest rainfall in August 2018 (Sudheer *et al.* 2019). The current investigation examines how climate change affects the streamflow from the Idamalayar catchment, Kerala, using a hydrological model.

2. STUDY AREA AND DATA USED

2.1. Study area

The river Idamalayar is a major tributary of the Periyar River. It originates from the Anamalai hills, located at an elevation of roughly 2,520 m in the Western Ghats of India. Anamalayar, Manaliyar, and several small streams join to form the river Idamalayar. The total length of river Idamalayar up to the confluence with the Periyar is 74 km. The watershed is located between latitudes 10°10′N and 10°20′N and longitude 76°20′E and 77°40′E. Figure 1(a) shows the location of the Idamalayar catchment. The total area of the Idamalayar catchment is 380.79 km^2, excluding the 101 km^2 catchment of Nirar that is diverted to Tamil Nadu. The catchment receives an average annual rainfall of about 475 cm. The annual average runoff from the catchment is 1,369.69 million m^3. The different land-use classes in the catchment are forest, water, and rangeland, as shown in Figure 1(b). The primary soil classes in the catchment are clayey loam and sandy clay loam, as shown in Figure 1(c).

2.2. Datasets

The development of hydrological models often requires spatial and temporal data (Luo *et al.* 2019; Haro-Monteagudo *et al.* 2020). The spatial data requirement includes topography, land use, and soil maps. The temporal data required include hydro-meteorological data. Table 1 shows the different datasets and their sources used for the current study.

2.2.1. Hydro-meteorological and geographical data

The daily meteorological data for 1987–2017 were collected from Indian Meteorological Department (IMD). The daily rainfall was acquired from IMD as 0.25 × 0.25° gridded data (Pai *et al.* 2014). The original resolution of daily temperature data was 1 × 1° (Srivastava *et al.* 2009). Using the bilinear interpolation, the daily temperature was regridded to 0.25 × 0.25° to match the grid points of rainfall data. The streamflow for 1987–2017 was collected from Kerala State Electricity Board (KSEB), Idamalayar division.

The geographical data used in this study include digital elevation model (DEM) data, soil data, and land-use data. The Cartosat DEM with a resolution of 30 m was obtained from Bhuvan. The elevation of the catchment varies from 53 to 2,575 m. The required land-use map was prepared from Landsat 8 images using the maximum likelihood classification tool in ArcMap. Training samples are created by visual inspection of the image. Signature file is created from these training samples and is used for classification. The primary land-use class in the catchment is forest (87.25%), followed by water (6.92%) and rangeland (5.83%). The required soil map was obtained from the Food and Agricultural Organization (FAO) of the United Nations. The soil classes in the study area include clayey loam (63.58%) and sandy clay loam (36.42%).

2.2.2. Bias-corrected climate data

The primary tools for deriving future climate data are the GCMs. Due to their coarse scale, GCMs intended to project climate data cannot be used directly at the regional and basin levels (Jaiswal *et al.* 2020). They must be downscaled to a fine resolution (Luo *et al.* 2019). Different statistical and dynamical methods are available for downscaling (Shaaban *et al.* 2011). Along with downscaling, bias correction must be done to eliminate the systematic error caused by the coarse resolution (Mishra *et al.* 2020a; Kim *et al.* 2022). Mishra *et al.* (2020a) downscaled precipitation and maximum and minimum temperatures from 13 GCMS using empirical quantile mapping and developed a dataset at a daily timescale at a spatial resolution of 0.25 × 0.25° for South Asia and 18 river basins of the Indian subcontinent. The bias-corrected dataset (Mishra *et al.* 2020b) from the 13 CMIP6 GCMs for the historical (1990–2014) and projected (2031–2040, 2051–2060, and 2071–2080) periods for the three SSP scenarios (SSP126, SSP245, and SSP585) are used in the present study.

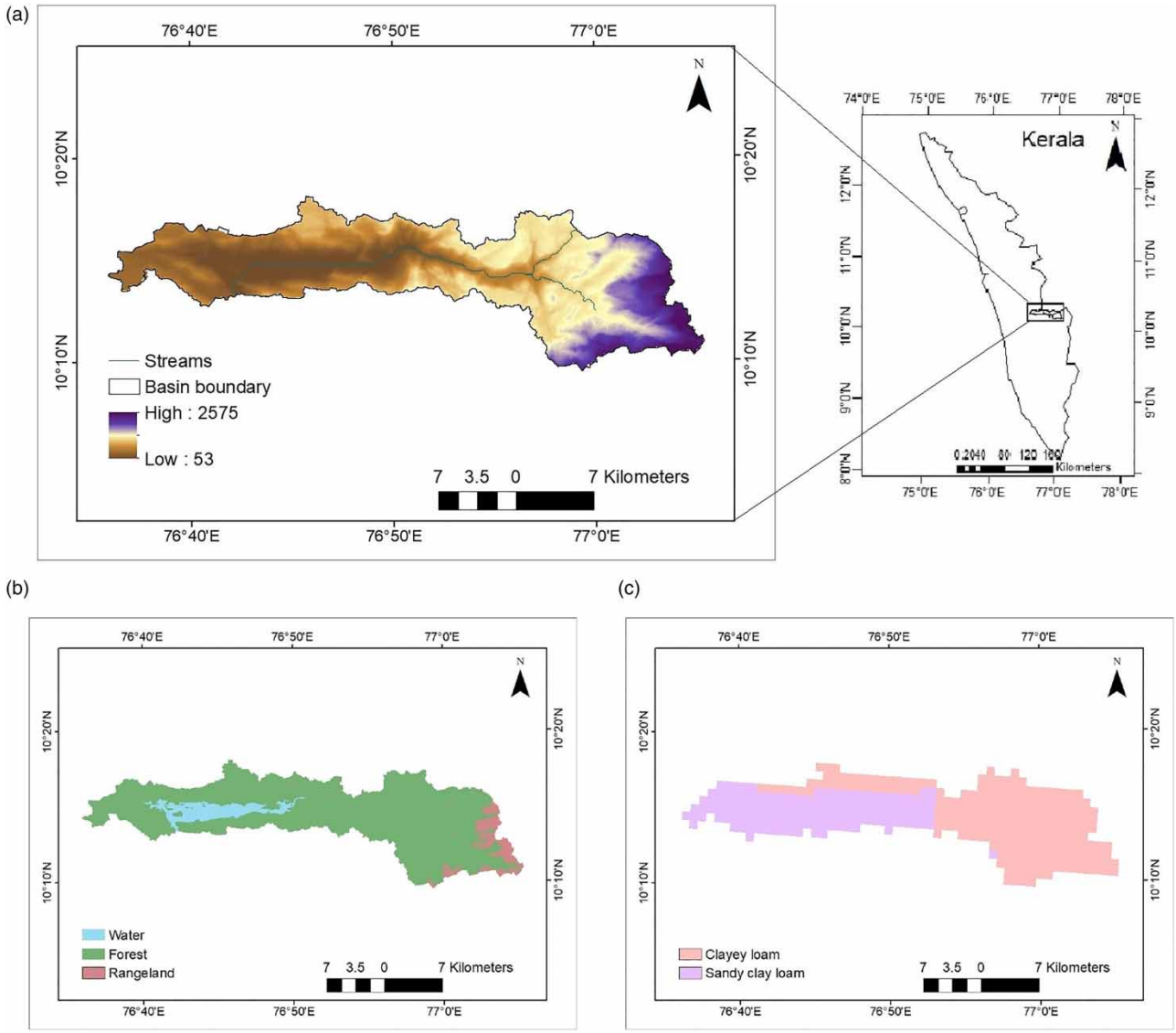

Figure 1 | (a) Location map and DEM, (b) land-use map, and (c) soil map of the Idamalayar catchment.

Table 1 | Sources and resolutions of data used

Data	Source	Resolution
DEM	Bhuvan (https://bhuvan.nrsc.gov.in)	30 m
Landsat 8 images (for developing land-use maps)	United States Geological Survey (https://earthexplorer.usgs.gov/)	30 m
Soil map	FAO of the United Nations (https://data.apps.fao.org/)	5 arc minutes
Precipitation	IMD (https://www.imdpune.gov.in)	0.25 × 0.25°
Maximum and minimum temperatures	IMD (https://www.imdpune.gov.in)	1 × 1°
Bias-corrected climate dataset (precipitation, maximum, and minimum temperatures)	Mishra *et al.* (2020b) https://zenodo.org/record/3987736	0.25 × 0.25°

3. METHODOLOGY

To comprehend the variation in water availability caused by climatic change, a hydrological model should be simulated for future scenarios. The methodology adopted in the present study is shown in Figure 2. In this study, two semi-distributed hydrological models, i.e., SWAT and HEC-HMS, are used for modelling the streamflow using the spatial and temporal data mentioned in Table 1. These two models were calibrated and validated against observed data. Then, the performance of the models was assessed using Nash–Sutcliffe efficiency (NSE), coefficient of determination (R^2), percentage bias (PBIAS), and root-mean-square error–standard deviation ratio (RSR). The model with better performance is further used for simulating the streamflow under climate change scenarios for three future periods, i.e., near-future (NF; 2031–2040), mid-future (MF; 2051–2060), and FF (2071–2080).

From the bias-corrected dataset, five GCMs are selected using a multicriterion decision-making method, the Preference Ranking Organisation Method of Enrichment Evaluation (PROMETHEE-2). The projected precipitation, maximum temperature, and minimum temperature GCM data are compared with the observed data of the baseline period (1990–2017) for this purpose. These projected climate data are input to the hydrological model to study the change in water availability in the Idamalayar basin. Finally, the output is used for frequency analysis to estimate streamflows for various return periods.

3.1. SWAT model

SWAT is a physically based, semi-distributed hydrological model widely used to study decadal changes through continuous simulation (Arnold *et al.* 1998). It requires geographical data, including DEM, soil map and land-use map, and hydro-meteorological data, including precipitation, maximum and minimum temperature, solar radiation (SR), wind speed (WS), and

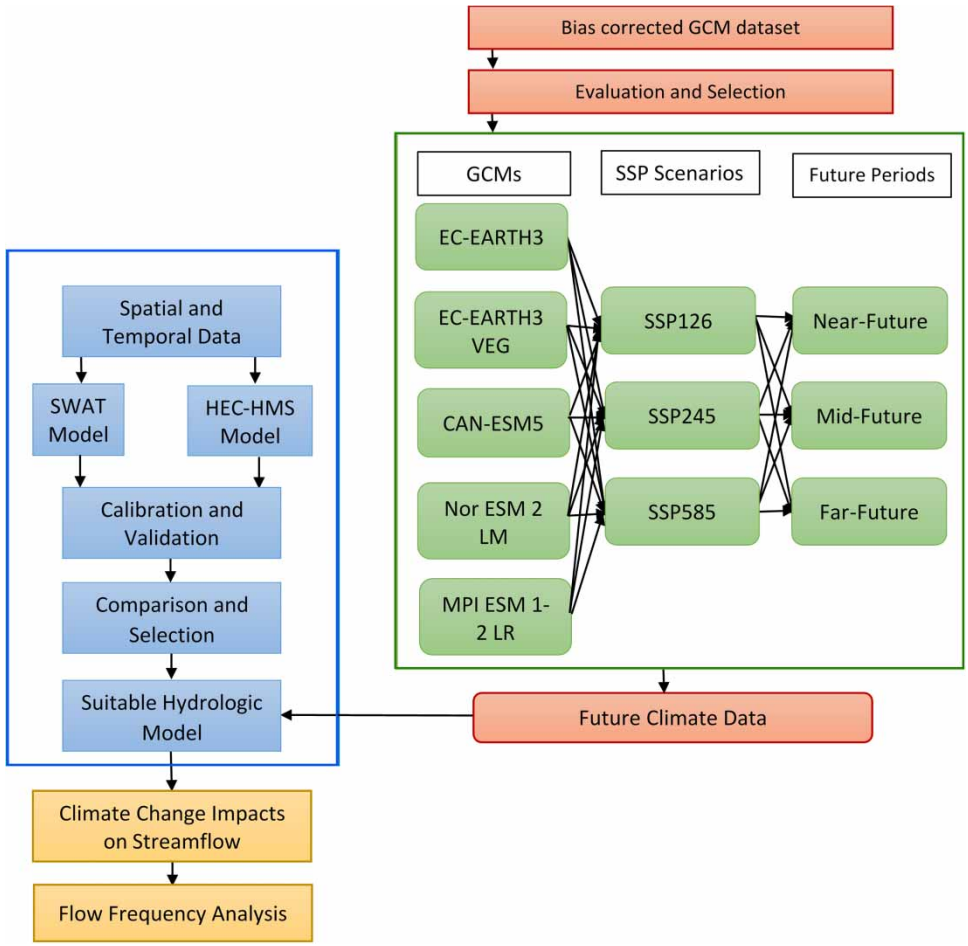

Figure 2 | Methodology of the present study.

relative humidity (RH) as input. In the absence of observed data, the built-in weather generator for SWAT is used to produce SR, WS, and RH (Neitsch *et al.* 2011; Zhang *et al.* 2016). This study used ArcSWAT 2012, an ArcGIS extension and graphical user interface for SWAT. In the SWAT model, the watershed is divided into sub-basins. Based on the land use, soil, and watershed slope, these sub-basins are further separated into homogeneous units known as HRUs. The water is routed through the channel network using variable storage routing method (Neitsch *et al.* 2011). The water balance equation is the fundamental equation that governs the SWAT model. It is given by Arnold *et al.* (1998) as shown in Equation (1):

$$\mathrm{SW}_t = \mathrm{SW}_0 + \sum_{i=1}^{t} (R_{\mathrm{day},i} - Q_{\mathrm{Surf},i} - E_{a,i} - W_{\mathrm{seep},i} - Q_{\mathrm{gw},i}) \tag{1}$$

where SW_0 represents the soil's initial water content and SW_t represents the soil's water content on day t. The equation deducts all types of water loss from the total amount of precipitation on day i, including surface runoff ($Q_{\mathrm{Surf},i}$), evapotranspiration ($E_{a,i}$), loss to the vadose zone ($W_{\mathrm{seep},i}$), and return flow ($Q_{\mathrm{gw},i}$) (Neitsch *et al.* 2011; Yaduvanshi *et al.* 2018; Gomes *et al.* 2021). All units are in millimetres of water. The runoff is provided in SWAT using the runoff curve number (CN) approach by the USDA Soil Conservation Service, as shown in Equation (2):

$$Q_{\mathrm{surf}} = \frac{(R_{\mathrm{day}} - I_a)^2}{(R_{\mathrm{day}} - I_a + S)} \tag{2}$$

where Q_{surf} is cumulative rainfall excess (i.e., runoff), R_{day} is the depth of the day's rainfall, and I_a is the initial abstraction, a function of infiltration, interception, and surface storage. S is the retention parameter estimated from the CN.

3.2. HEC-HMS model

The US Army Corps of Engineers (USACE) developed the HEC-HMS model to route a runoff hydrograph through a stream network and calculate watershed discharge over time (USACE 2018). It is widely used for event as well as continuous simulations. A control specification, a meteorological model, and a basin model make up a typical HEC-HMS project. The time constraints of the model are specified in the control specification. The basin's rainfall is given using the meteorological model. The basin model represents the physical watershed with the help of hydrologically related stream reaches, sub-basins, and junctions.

In the present study, the deficit and constant loss method is used to model the infiltration losses, and the Clark unit hydrograph method is used to compute direct runoff. The recession model is employed to model baseflow, and the Muskingum routing model is used to simulate the streamflow in the reaches.

These two models are used for simulating the daily streamflow from the Idamalayar River Basin. In the SWAT model, the simulation is carried out from 1987 through 2017. In HEC-HMS, the simulation is carried out from 1990 to 2017. The change in the start date of simulation in the two models is due to the application of a warm-up period of 3 years in SWAT.

3.3. Calibration and validation of the models

Model calibration is the process of adjusting the model parameters so that the simulated output matches the observed data. For the automatic calibration and validation of SWAT, a standalone tool named SWAT-Calibration and Uncertainty Program (SWAT-CUP) is used. SWAT-CUP provides different options from which the Sequential Uncertainty Fitting Algorithm (SUFI-2) is employed in the current study. Along with auto-calibration, the SUFI-2 algorithm ranks the significant parameters with respect to their sensitivity (Bhatta *et al.* 2019). Detailed information regarding SWAT-CUP and SUFI-2 algorithm is available in the study by Abbaspour (2012). The HEC-HMS model supports manual calibration in addition to its auto-calibration system. In the present study, the models were calibrated for a daily time scale from 1990 through 2007 and validated for 2008–2017 using the respective methods.

3.4. Evaluation of the performance of the models

The efficacy of the models was evaluated using four goodness-of-fit measures, i.e., R^2, NSE, PBIAS, and RSR. R^2 ranges from 0 to 1, with 1 denoting the ideal value. Another performance measure is NSE, which describes the relative magnitude of the residual variance compared to the variance of the observed data as a range between $-\infty$ and 1.0, with 1 denoting the ideal

value. An NSE greater than 0.50 is considered to be satisfactory for a daily time scale model, according to Moriasi *et al.* (2007). PBIAS measures the simulated data's average tendency to be larger or smaller than their observed counterparts (Moriasi *et al.* 2007). The optimal value of PBIAS is zero. Positive values of PBIAS indicate model underestimation bias and a negative value indicates an overestimation bias. Singh *et al.* (2005) have recommended another model evaluation statistic, i.e., RSR. The lower the RSR, the better the model's performance.

3.5. GCM evaluation and selection

The best five GCMs are selected based on several performance measures from the bias-corrected dataset using multicriterion analysis, PROMETHEE-2. Raju & Nagesh Kumar (2020) describe many performance metrics used to rate GCMs in various studies conducted worldwide. The current study chose four performance indices: R, NSE, normalized root-mean-square error (NRMSE), and the absolute normalized mean bias error (ANMBE) to evaluate the GCM and rank them. The value of R shows the linear correlation between observed and projected data, ranging from -1 to 1. A positive R indicates a strong correlation, and a negative R implies a weak correlation. NRMSE determines the similarity of the two time series by considering mean and standard deviation. It is defined as the root-mean-square error divided by the corresponding standard deviation of the observed field. Smaller values of NRMSE imply better model performance. Ideally, a value of 0 is preferred. ANMBE is the ratio of the mean difference between the observed and projected values to the mean of observed values. A small value of ANMBE is preferred.

The entropy method, which has the advantage of reducing the bias to any indicator, was used to determine the weight of the indicators for each climate variable (Raju & Kumar 2014). Then the PROMETHEE-2 method was applied to find the net ranking of each GCM based on each climate variable. The overall ranking of the GCMs is found by adding the net ranking indices by giving weight to each climate variable (0.5 for precipitation and 0.25 each for maximum temperature and minimum temperatures).

3.6. Changes in precipitation, temperature, and streamflow

The best five GCMs performed well in describing the historical precipitation and temperature are identified. The climatic variables for the future period are obtained using these five GCMs. The changes in climatic variables for three future periods, say, NF, MF, and FF, are analysed against the baseline scenario (1990–2017). The analysis is carried out for three SSP scenarios, i.e., SSP126, SSP245, and SSP585.

Using the projected climatic variables for the five GCMs, under three scenarios, the streamflow from the river basin is simulated for three future periods. This simulated output is then compared to the streamflow for the baseline scenario to understand the impact of climate change on water availability in the river basin.

3.7. Flow frequency analysis

Generalized extreme value (GEV) distribution is utilized for flow frequency analysis. GEV is a combination of three distributions, i.e., Gumbel, Frechet, and Weibul distributions, and is widely used for flow frequency analysis (Mandal & Simonovic 2017). The flow frequency analysis is conducted utilizing the *ismev* package in RStudio (Coles 2001).

4. RESULTS AND DISCUSSIONS

4.1. Hydrologic modelling

The values of the performance indices for calibration and validation of the hydrological models (SWAT and HEC-HMS) are given in Table 2. The simulated streamflows for both models matched the observed flows satisfactorily. The R^2 values were found to be 0.64 and 0.75 in calibration and validation for SWAT. For HEC-HMS, the R^2 values were 0.54 and 0.68 for calibration and validation, respectively. The NSE values for calibration were 0.61 and 0.51 for SWAT and HEC-HMS, respectively. The same for validation were 0.67 and 0.58. The values of all the indicators were better for SWAT than HEC-HMS, in both calibration and validation. Figure 3(a)–3(d) compares observed and model-simulated flows for calibration and validation.

Figure 3(a) and 3(b) shows that both models captured the low and peak flows satisfactorily. In addition, both models perform well in capturing the flow pattern. But while comparing the performance of the models, it was observed that the values of evaluation indices were higher for the SWAT model, which reflects the suitability of the SWAT model over the HEC-HMS

Table 2 | Performance indicators for SWAT and HEC-HMS for calibration and validation

	Performance indicator							
	R^2		NSE		PBIAS		RSR	
Hydrologic model	Calibration	Validation	Calibration	Validation	Calibration	Validation	Calibration	Validation
SWAT	0.64	0.75	0.61	0.67	22.50	36.90	0.63	0.58
HEC-HMS	0.54	0.68	0.51	0.58	− 26.56	− 38.06	0.70	0.60

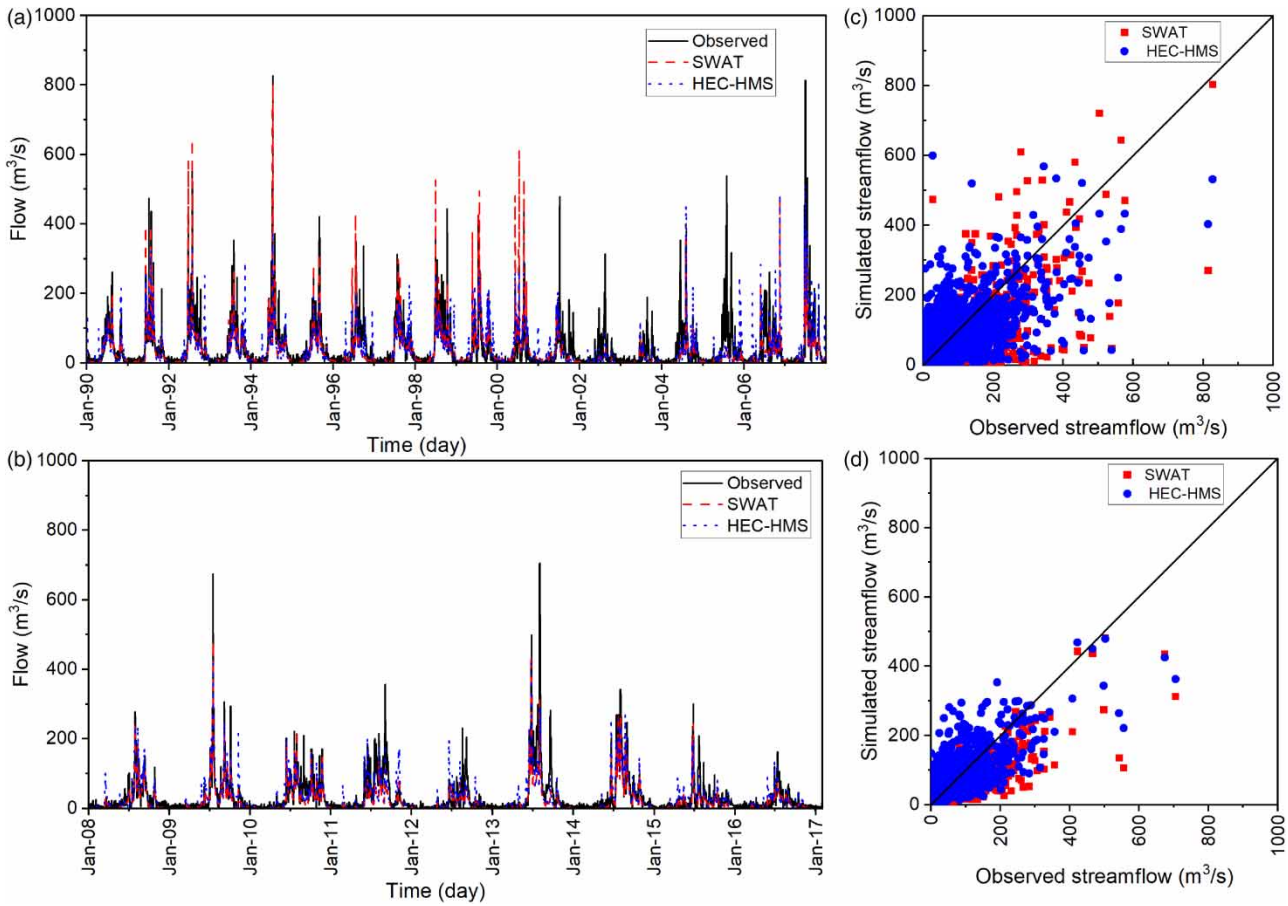

Figure 3 | (a) and (b) Comparison of observed and simulated streamflows from Idamalayar River Basin during calibration and validation; and (c) and (d) scatter plot of simulated and observed streamflows for calibration and validation.

model in reproducing the observed streamflow from the Idamalayar catchment. Hence, the SWAT model was used for simulating the streamflow for future periods under climate change conditions.

4.2. Ranking of GCMs

The results of the ranking of 13 GCMs are presented in Table 3. Based on the ranking, the top five GCMs, namely, EC-EARTH3, EC-EARTH3 VEG, CAN-ESM5, Nor ESM 2 LM, and MPI ESM 1-2 LR, were used in the study for further analysis. These will be called GCM1, GCM2, GCM3, GCM4, and GCM5. The future climatic data, including precipitation, maximum temperature, and minimum temperature from these five GCMs, were analysed and compared to those in the baseline scenario (1990–2017). The calibrated hydrologic model used outputs from these five GCMs to simulate future Idamalayar streamflow.

Table 3 | Net ranking index and rank of the selected GCMs

Model no.	Model	Net ranking index				Rank
		Precipitation	Maximum temperature	Minimum temperature	Total ranking index	
1	ACCESS-CM2	− 0.062	− 0.467	− 0.485	− 0.269	10
2	ACCESS-ESM1-5	− 0.140	0.216	− 0.630	− 0.173	9
3	BCC-CSM2-MR	− 0.212	− 0.818	0.811	− 0.108	8
4	CanESM5	− 0.484	0.816	1.000	0.212	3
5	EC-Earth3	0.647	0.784	0.504	0.646	1
6	EC-Earth3-Veg	0.438	0.597	0.330	0.451	2
7	INM CM4-8	− 0.103	− 0.402	− 0.976	− 0.396	13
8	INM CM5-0	− 0.096	− 0.150	− 0.825	− 0.291	12
9	MPI-ESM1-2-HR	− 0.654	0.329	− 0.154	− 0.283	11
10	MPI-ESM1-2-LR	− 0.121	0.118	0.634	0.127	5
11	MRI-ESM2-0	− 0.412	0.350	0.162	− 0.078	7
12	NorESM2-LM	0.686	− 0.758	− 0.026	0.147	4
13	NorESM2-MM	0.510	− 0.616	− 0.344	0.015	6

4.3. Projected change in climate

The variations of precipitation (%) and maximum and minimum temperatures (°C) across GCMs compared to the baseline period are shown in Figure 4(a)–4(i). Under SSP126, in the NF period, the variation of precipitation from the baseline scenario varies between an increase of 13.9% and a decrease of 5.8%, with a median lying at an increase of 3.1%. Similarly, the median value for the MF period lies at 3.4%, and that of the FF period lies at −1.2%, the negative sign implying a decrease. The variation across GCMs is higher for the MF period compared to NF and FF periods, as shown in Figure 4(a).

Regarding the NF period of SSP245, the change in precipitation from the baseline period ranges from −17.5 to 6.8%, with the median lying at 2.8%. For the MF period under SSP585, the median lies at 2.3%. For the FF period, the median lies at 2.2%, with variations ranging from −20.3 to 7.3%. For all three future periods, the median lies around 2%, as shown in Figure 4(b).

While observing the box plots for the NF period under SSP585, it can be seen that the change in precipitation compared to the baseline period varies from −6.8 to 22.1%, with the median at 2.2%. For the MF period, the median lies at 5.2%. In addition, the range of variation is higher, which extends up to a 47% increase. The same pattern can be observed in the case of the FF period under the same scenario, with the median lying at 15% and the highest variation ranging up to 75%.

As shown in Figure 4(d), the decrease in maximum temperature in the NF period under SSP126 ranges from 2.04 to 2.95 °C with the median at 2.81 °C. Similarly, for the MF period, the median lies at 2.55 °C, and for the FF period, it lies at 2.52 °C. Under SSP245, in the NF period, the decrease ranges from 2.11 to 3.09 °C with the median at 2.76 °C. For the MF period, the range lies between 1.57 and 2.65 °C, with the median at 2.42 °C. For the FF period, median is at 2.16 °C. It is observed that the average decline across GCMs is higher in the NF period, which decreases in the MF period and further decreases in the FF period. A similar pattern can be observed under the SSP585 scenario. The median decreases across GCMs are 2.72, 2.19, and 1.78 °C for NF, MF, and FF periods, respectively. While observing the changes in monthly maximum temperature, it was found that generally, the decrease in temperature is higher during monsoon months (June–September) and lesser during summer months (February–May).

When analysing the changes in the average annual minimum temperature, patterns resembling those of the annual maximum average temperature were seen (Figure 4(g)–4(i)). The decrease from the baseline period tends to reduce in MF and FF periods compared to that in the NF period. This observation is also similar to the case of average annual maximum temperature. Similar tendencies to those of the monthly average maximum temperature were seen while taking the change in monthly average minimum temperature into account. While observing the monthly minimum temperature, the same pattern was seen as that of the monthly maximum temperature.

The projected monthly average precipitation is compared under three SSP scenarios for five GCMs and three future periods in Figure 5(a)–5(i). A significant shift in the pattern of precipitation is observed in most cases. The peak precipitation in the baseline scenario is observed in the month of July. In the projected scenarios, the presence of an alternate peak can be

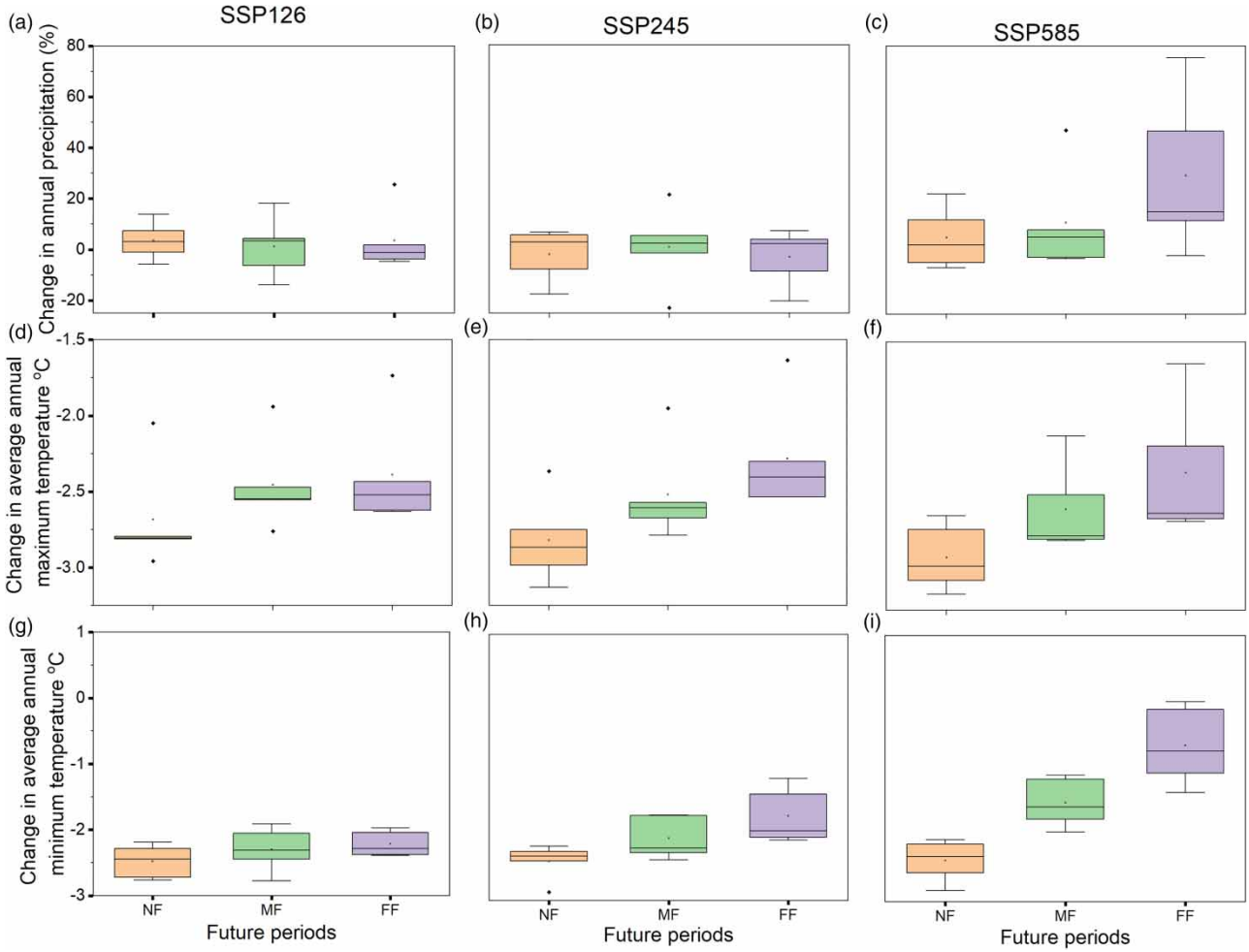

Figure 4 | Box plots: projected change in annual precipitation under (a) SSP126, (b) SSP245, and (c) SSP585, projected change in annual average maximum temperature under (d) SSP126, (e) SSP245, and (f) SSP585, and projected change in annual average minimum temperature under (g) SSP126, (h) SSP245, and (i) SSP585.

observed in the month of October. Another important observation is that in most of the cases, the peak observed in October is higher compared to that in July. That means a change in peak is also observed along with the formation of an alternate peak. Except for GCM4, a shift in peak from July to October, that is, the shift in peak from south-west monsoon (which starts from June and ends in September) to north-east monsoon (which begins in October and ends in November) is observed in all the scenarios for all three future periods. For instance, the projection of precipitation by GCM5 in the FF period under SSP585 (Figure 5(i)) clearly indicates the presence of another peak in October, which is higher in magnitude than that in July.

Comparing the projected climate variables to the baseline scenario gave essential insights regarding the future climate of the Idamalayar catchment. A slight increase in average annual precipitation is observed in some instances. A shift in the peak rainfall from July to October is also observed in most cases. It was also found that the average annual maximum and minimum temperatures are decreasing except in a few instances. The monthly variation of all these variables varies from GCM to GCM and in various SSP scenarios. These variations in climate variables will be reflected in the water availability in the river basin discussed in the following section.

4.4. Hydrologic response to changing climate

Figure 6(a)–6(c) shows the box plot for change in annual streamflow from the baseline scenario for the three SSP scenarios. As observed in Figure 6(a), for the NF period, the decrease in streamflow ranges from 19.05 to 45.03%, with the median lying

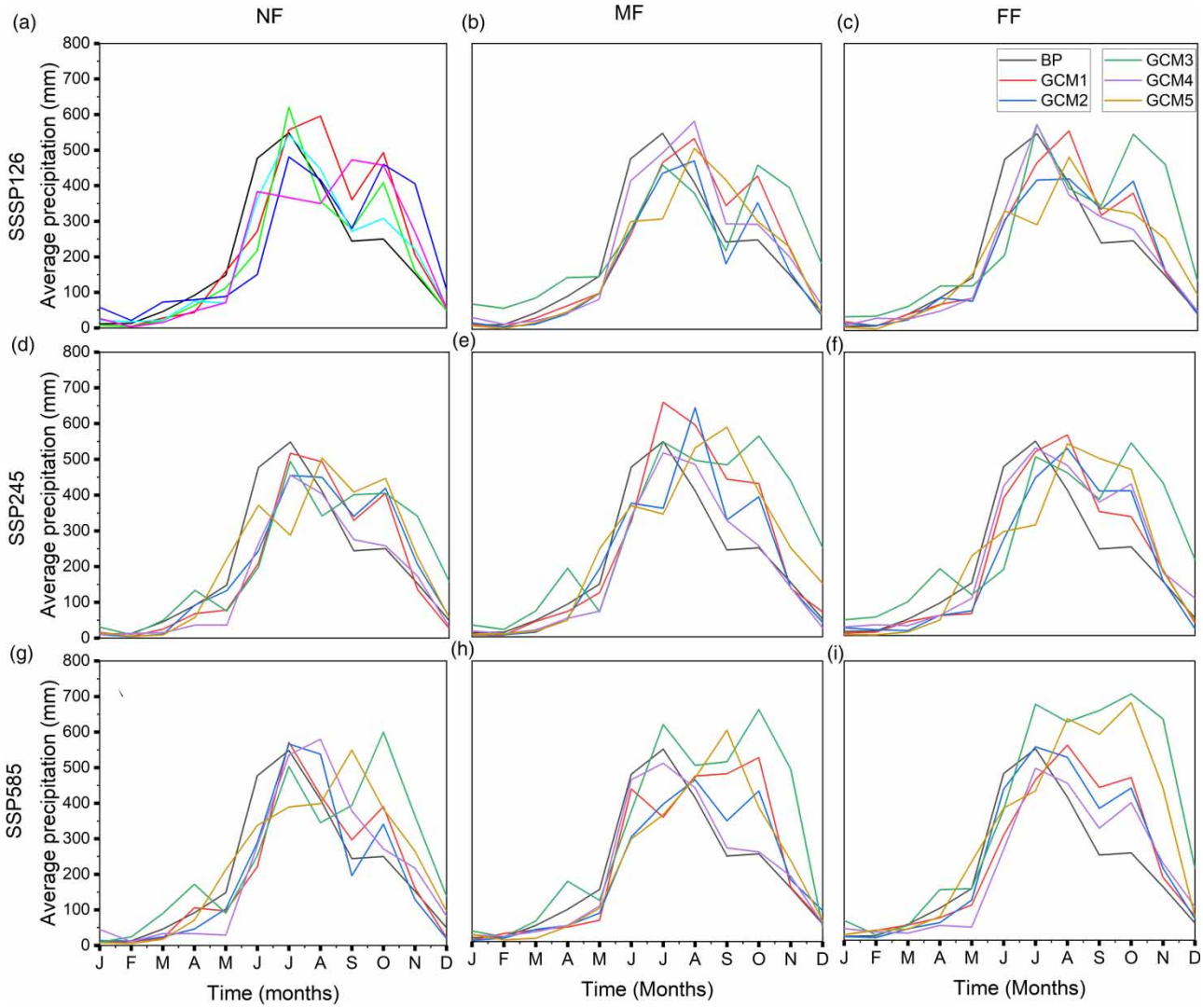

Figure 5 | (a–i) Comparison of projected monthly average precipitation with that of the baseline period (BP).

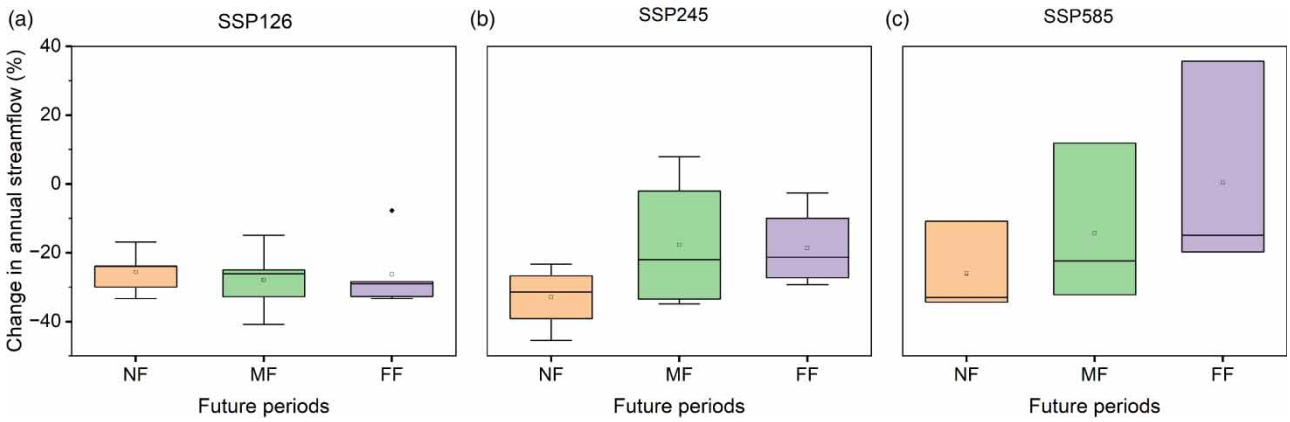

Figure 6 | Box plot for change in annual streamflow (%) from the baseline scenarios for (a) SSP126, (b) SSP245, and (c) SSP585.

Table 4 | Historical and future mean seasonal flows (MCM) for different SSP scenarios in the Idamalayar river basin

		Near future				Mid future				Far future			
SSP scenarios	Historical	25th percentile	50th percentile	75th percentile	Change in median value (%)	25th percentile	50th percentile	75th percentile	Change in median value (%)	25th percentile	50th percentile	75th percentile	Change in median value (%)
SSP126													
Yearly	1,173.18	821.64	891.31	892.52	– 24.03	788.24	866.98	879.88	– 26.10	788.86	832.97	840.11	– 29.00
S-W monsoon	874.56	440.23	449.75	485.18	– 48.57	412.24	438.24	485.59	– 49.89	435.58	452.31	477.28	– 48.28
N-E monsoon	181.11	219.48	226.89	305.45	25.28	219.30	235.33	264.61	29.93	227.60	237.71	238.80	31.25
Winter	49.39	101.93	102.93	121.29	108.40	95.80	96.17	108.07	94.71	86.86	86.90	113.24	75.95
Summer	68.12	14.82	25.81	27.10	– 62.11	14.70	18.87	20.62	– 72.30	23.28	28.67	46.28	– 57.90
SSP245													
Yearly	1,173.18	788.01	820.06	899.05	30.10	797.84	1,032.85	1,063.68	– 11.96	876.39	929.85	970.07	– 20.74
S-W monsoon	874.56	410.33	439.93	455.60	– 49.70	490.00	544.26	560.94	– 37.77	482.83	485.11	546.76	– 44.53
N-E monsoon	181.11	187.44	248.47	281.77	37.19	213.40	255.70	299.77	41.18	243.01	270.80	302.04	49.52
Winter	49.39	83.17	99.92	110.56	102.31	95.71	98.12	152.35	98.67	88.34	96.20	124.21	94.78
Summer	68.12	18.52	31.73	42.36	– 53.41	28.24	30.96	67.30	– 54.55	16.93	28.30	46.51	– 58.45
SSP585													
Yearly	1,173.18	786.03	859.39	972.12	– 26.75	813.66	899.75	910.59	– 23.31	941.22	997.63	1,322.50	– 14.96
S-W monsoon	874.56	457.82	489.81	504.11	– 43.99	487.10	516.66	517.28	– 40.92	523.52	594.03	638.43	– 32.08
N-E monsoon	181.11	220.62	231.36	288.61	27.74	253.99	279.65	285.04	54.40	270.11	277.84	458.39	53.41
Winter	49.39	77.40	110.47	125.64	123.68	99.87	106.67	116.76	115.98	109.11	127.89	163.09	158.93
Summer	68.12	18.04	30.19	53.76	– 55.67	18.17	20.93	68.96	– 69.27	20.93	24.39	62.59	– 64.19

at −32.65 (negative sign indicating a decrease). Similarly, in the MF period, the variation ranges from −21.33 to −44.12%, with the median at −30.41%. Again, for the FF scenario, the median lies at 28.93%.

In the case of the SSP245 scenario, for the NF period, the variation ranges between −21.91 and −44.35%, with the median at 27.58%. The median changes for the MF and FF periods lie at −29.64 and −28.72%. For the SSP585 scenario, in the NF period, the variation of streamflow from the baseline period ranges between −17.46 and −42.07%, with the median lying at −36.58%. At the same time, for the MF period, the range of variation extends between −16.75 and −44.11%. The median of the same lies at −30.59%. In the case of the FF period, the median lies at −21.90%. Figure 6(a)–6(c) shows that the extent of variation of streamflow from the baseline scenario across GCMs gets higher in the SSP585 scenario. The variation was lesser for the SSP126 scenario. Generally, the average annual streamflow is found to be decreasing. Similar results were also reported by Sadhwani *et al.* (2023), stating that there are more possibilities of a decrease in the average annual streamflow.

While comparing the average change in annual streamflow for the three SSP scenarios, it was observed that the decrease is highest under the SSP126 scenario and least under the SSP585 scenario. The comparison of average annual flows (historical and projected) is shown in Table 4. The results indicate a decline in the projected average annual flow. In addition, the comparison of average historical and future seasonal flows is also shown in Table 4. It shows that the flow during the south-west monsoon decreases by 48.57%, whereas the flow during the north-east monsoon increases by 25.28% in the NF period under

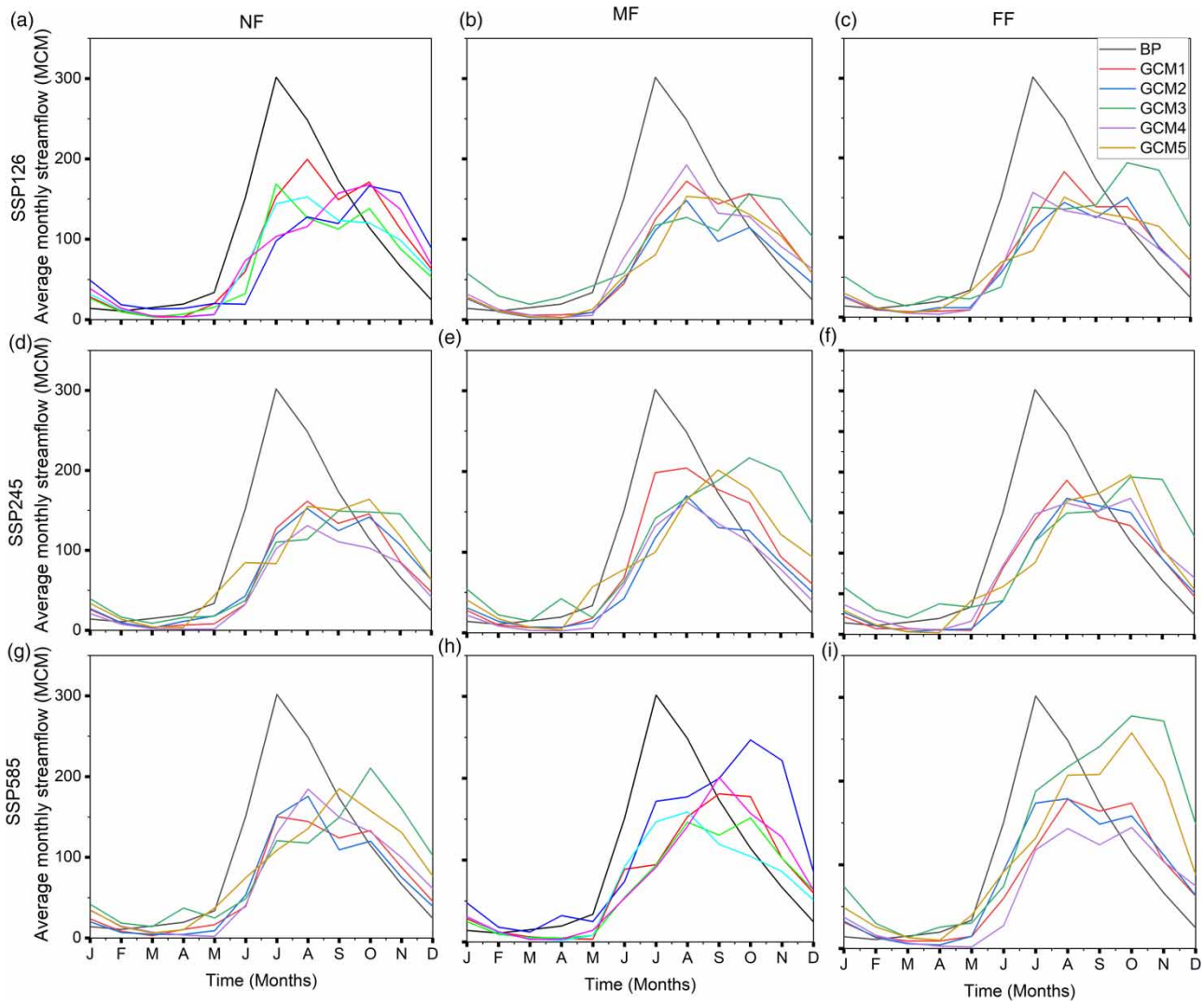

Figure 7 | (a–i) Comparison of monthly average streamflow with that of the baseline period.

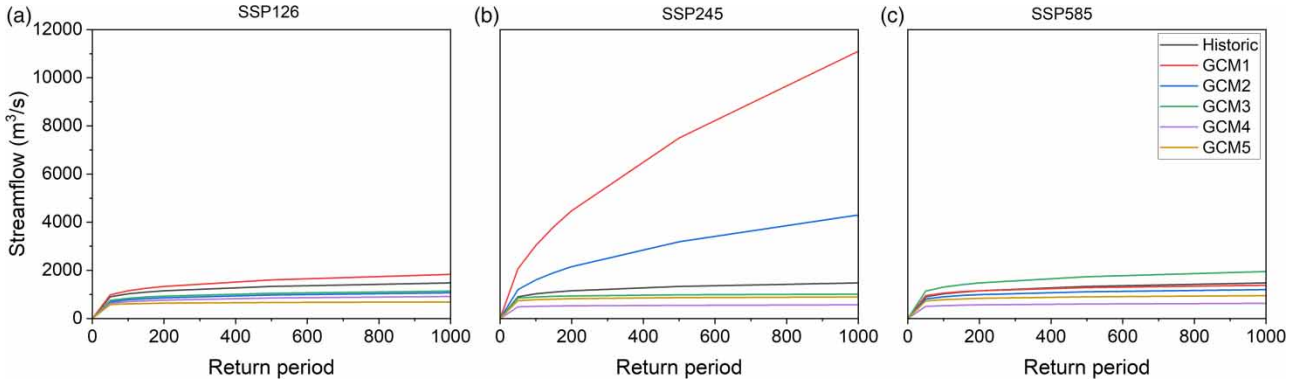

Figure 8 | (a–c) Results of flow frequency analysis of Idamalayar River Basin using GEV for different SSP scenarios.

the SSP126 scenario. The winter (December–February) flow increases by 108.40%, and the summer (March–May) flow is expected to decrease by 62.11%. This pattern of a decrease in flow during the south-west monsoon and summer and an increase during the north-east monsoon and winter seasons was observed for different future periods and SSP scenarios.

The variation of average monthly streamflow under the three scenarios for three future conditions for the five GCMs is shown in Figure 7(a)–7(i). Similar to precipitation, the peak in the flow during the baseline period is observed in July. Figure 7(a)–7(i) shows that, along with the peak in July, an alternate peak is seen during October. This shift in pattern is visible across all GCMs except GCM4. In most cases, the peak in October is higher than that in July. This indicates a profound shift in the flow pattern across months. The peak is delayed and shifted from July to October, i.e., from the south-west monsoon to the north-east monsoon. Another important observation is the decline in peak. The variation from baseline scenarios is profound in the case of non-monsoon months also. The variation is different across GCMs. For example, in the case of GCM3, a significant shift in peak can be observed. At the same time, for GCM4, the baseline pattern of the peak in July is reproduced. So, from the results, it is clear that the streamflow pattern variation is substantial in the case of monthly flows.

4.5. Results of flow frequency analysis

The results of flow frequency analysis for different future scenarios are shown in Figure 8. The flow frequency curve for the future periods is compared to that of the baseline scenario in Figure 8(a)–8(c). It can be seen from Figure 8 that the predicted streamflow corresponding to different return periods varies across GCMs for the three scenarios. The variation is profound in the case of SSP245. The flows corresponding to different return periods are higher for GCM1 and GCM2 under SSP126. For SSP245, very high flows for different return periods are observed for GCM1 and GCM2, whereas, in the case of SSP585, all the curves except GCM3 show less flows corresponding to different return periods.

5. CONCLUSIONS

This study investigated the impact of climate change on the streamflow from the Idamalayar catchment. The efficiencies of two hydrologic models, i.e., SWAT and HEC-HMS, were assessed using four performance indicators. SWAT, which outperformed HEC-HMS in simulating the Idamalayar streamflow, was selected for further simulations. A multicriterion analysis (PROMETHEE-2) was used for ranking the GCMs. The changes in climatic variables such as precipitation, maximum temperature, and minimum temperature were analysed for three future periods, say, NF, MF, and FF, under three SSP scenarios, i.e., SSP126, SSP245, and SSP585.

The precipitation projections for the three SSP scenarios and future periods were observed to be different for all five GCMs. Under SSSP126, the average percentage change in annual precipitation for the five GCMs is positive (3.52%) in the NF period. It becomes negative in MF and FF periods (−1.16 and −3.57%, respectively). Under SSP245, the average change in precipitation is negative (−2.12%) in the NF period, while in the MF and FF, it is positive (16.06 and 11.09%, respectively). Under SSP585, precipitation is expected to increase in all future periods.

The maximum temperature shows a decreasing trend in the projections in all cases. The average change ranges from 2.38 to 2.68 °C under the SSP126 scenario. The decrease in maximum temperature under SSP245 scenarios ranges from 2.0 to 2.7 °C. In the case of the SSP585 scenario, this range lies between 1.13 and 2.71 °C. The smallest decline in maximum temperature

happens under SSP585, while the highest decrease occurs under SSP126. Similar observations were found for minimum temperature. Generally, the minimum temperature decreases, with the highest and lowest declines projected under SSP126 and SSP585, respectively.

These outputs from the five GCMs were used to simulate the streamflow from the catchment. In general, it has been observed that the streamflow decreases in the future for different scenarios. An exception was observed for GCM3 under the SSP585 scenario. Under the SSP126 scenario, the average decline is around 26.6%, and the values are 21.94 and 9.24% for SSP245 and SSP585, respectively. Also, the peak flow shifts from July to October, i.e., from the south-west monsoon to the north-east monsoon, similar to precipitation. Frequency analysis showed that the variation of flows for different return periods is significant in the case of SSP245, in which outputs of GCM1 produced high flows.

In conclusion, the results indicate that the water availability in the Idamalayar basin will reduce in the future under the three SSP scenarios. There is a significant change in the flow pattern also. Both these necessitate the need for better management plans for the future. The analysis of the impact of climate change in the present study was limited to a particular region of Kerala. This can be extended to other river basins as well. Another vital area to be addressed is revisiting the rule curves of the Idamalayar reservoir, which will help to deal with the climate change impact on streamflow.

DATA AVAILABILITY STATEMENT

Data cannot be made publicly available; readers should contact the corresponding author for details.

CONFLICT OF INTEREST

The authors declare there is no conflict.

REFERENCES

Abbaspour, K. C. 2012 *SWAT Calibration and Uncertainty Program – A User Manual*. Swiss Federal Institute of Aquatic Science and Technology, Dübendorf.

Abdulahi, S. D., Abate, B., Harka, A. E. & Husen, S. B. 2022 Response of climate change impact on streamflow: the case of the Upper Awash sub-basin, Ethiopia. *Journal of Water and Climate Change* **13**, 607–628. https://doi.org/10.2166/wcc.2021.251.

Arnold, J. G., Srinivasan, R., Muttia, R. S. & Williams, R. 1998 Large area hydrologic modeling and assessment part I: model development. *Journal of the American Water Resources Association* **34**, 73–89.

Bhatta, B., Shrestha, S., Shrestha, P. K. & Talchabhadel, R. 2019 Evaluation and application of a SWAT model to assess the climate change impact on the hydrology of the Himalayan River Basin. *Catena* **181**, 104082. https://doi.org/10.1016/j.catena.2019.104082.

Bisht, D. S., Mohite, A. R., Jena, P. P., Khatun, A., Chatterjee, C., Raghuwanshi, N. S., Singh, R. & Sahoo, B. 2020 Impact of climate change on streamflow regime of a large Indian river basin using a novel monthly hybrid bias correction technique and a conceptual modeling framework. *Journal of Hydrology* **590**, 125448. https://doi.org/10.1016/j.jhydrol.2020.125448.

Coles, S. 2001 *An Introduction to Statistical Modeling of Extreme Values*. Springer, London.

Gao, D., Chen, T., Yang, K., Zhou, J. & Ao, T. 2021 Projecting the impacts of climate change on streamflow in the upper reaches of the Yangtze river basin. *Journal of Water and Climate Change* **12**, 1724–1743. https://doi.org/10.2166/wcc.2020.082.

Gomes, L. C., Bianchi, F. J. J. A., Cardoso, I. M., Schulte, R. P. O., Fernandes, R. B. A. & Fernandes-Filho, E. I. 2021 Disentangling the historic and future impacts of land use changes and climate variability on the hydrology of a mountain region in Brazil. *Journal of Hydrology* **594**, 125650. https://doi.org/10.1016/j.jhydrol.2020.125650.

Haro-Monteagudo, D., Palazón, L. & Beguería, S. 2020 Long-term sustainability of large water resource systems under climate change: a cascade modeling approach. *Journal of Hydrology* **582**, 124546. https://doi.org/10.1016/j.jhydrol.2020.124546.

Hunt, K. M. R. & Menon, A. 2020 The 2018 Kerala floods: a climate change perspective. *Climate Dynamics* **54**, 2433–2446. https://doi.org/10.1007/s00382-020-05123-7.

Jaiswal, R. K., Lohani, A. K. & Tiwari, H. L. 2020 Development of framework for assessment of impact of climate change in a command of water resource project. *Journal of Earth System Science* **129**, 58. https://doi.org/10.1007/s12040-019-1328-x.

Kim, K. B., Kwon, H. H. & Han, D. 2022 Intercomparison of joint bias correction methods for precipitation and flow from a hydrological perspective. *Journal of Hydrology* **604**, 127261. https://doi.org/10.1016/j.jhydrol.2021.127261.

Kumar, N., Tischbein, B., Kusche, J., Laux, P., Beg, M. K. & Bogardi, J. J. 2017 Impact of climate change on water resources of upper Kharun catchment in Chhattisgarh, India. *Journal of Hydrology: Regional Studies* **13**, 189–207. https://doi.org/10.1016/j.ejrh.2017.07.008.

Luo, M., Liu, T., Meng, F., Duan, Y., Bao, A., Xing, W., Feng, X., De Maeyer, P. & Frankl, A. 2019 Identifying climate change impacts on water resources in Xinjiang, China. *Science of the Total Environment* **676**, 613–626. https://doi.org/10.1016/j.scitotenv.2019.04.297.

Mandal, S. & Simonovic, S. P. 2017 Quantification of uncertainty in the assessment of future streamflow under changing climate conditions. *Hydrological Processes* **31**, 2076–2094. https://doi.org/10.1002/hyp.11174.

Mishra, V., Bhatia, U. & Tiwari, A. D. 2020a Bias-corrected climate projections for South Asia from coupled model intercomparison project-6. *Scientific Data* **7**, 338. https://doi.org/10.1038/s41597-020-00681-1.

Mishra, V., Bhatia, U. & Tiwari, A. D. 2020b Bias corrected climate projections from CMIP6 models for Indian sub-continental river basins [Data set]. Zenodo. https://doi.org/10.5281/zenodo.3987736.

Moriasi, D. N., Arnold, J. G., Van Liew, M. W., Bingner, R. L., Harmel, R. D. & Veith, T. L. 2007 Model evaluation guidelines for systematic quantification of accuracy in watershed simulations. *Transactions of the ASABE* **50**, 885–900. https://doi.org/10.13031/2013.23153.

Mudbhatkal, A., Raikar, R. V., Venkatesh, B. & Mahesha, A. 2017 Impacts of climate change on varied river-flow regimes of southern India. *Journal of Hydrologic Engineering* **22**, 05017017. https://doi.org/10.1061/(asce)he.1943-5584.0001556.

Neitsch, S., Arnold, J., Kiniry, J. & Williams, J. 2011 *Soil & Water Assessment Tool Theoretical Documentation Version 2009*. Texas Water Resources Institute, Texas. https://doi.org/10.1016/j.scitotenv.2015.11.063.

Oleyiblo, J. O. & Li, Z. J. 2010 Application of HEC-HMS for flood forecasting in Misai and Wan'an catchments in China. *Water Science and Engineering* **3**, 14–22. https://doi.org/10.3882/j.issn.1674-2370.2010.01.002.

Pai, D. S., Sridhar, L., Rajeevan, M., Sreejith, O. P., Satbhai, N. S. & Mukhopadhyay, B. 2014 Development of a new high spatial resolution (0.25° × 0.25°) long period (1901–2010) daily gridded rainfall data set over India and its comparison with existing data sets over the region. *Mausam* **65**, 1–18.

Palacios-Cabrera, T., Valdes-Abellan, J., Jodar-Abellan, A. & Rodrigo-Comino, J. 2022 Land-use changes and precipitation cycles to understand hydrodynamic responses in semiarid Mediterranean karstic watersheds. *Science of the Total Environment* **819**, 153182. https://doi.org/10.1016/j.scitotenv.2022.153182.

Pramanick, N., Acharyya, R., Mukherjee, S., Mukherjee, S., Pal, I., Mitra, D. & Mukhopadhyay, A. 2022 SAR based flood risk analysis: a case study Kerala flood 2018. *Advances in Space Research* **69**, 1915–1929. https://doi.org/10.1016/j.asr.2021.07.003.

Raju, K. S. & Kumar, D. N. 2014 Ranking of global climate models for India using multicriterion analysis. *Climate Research* **60**, 103–117. https://doi.org/10.3354/cr01222.

Raju, K. S. & Nagesh Kumar, D. 2020 Review of approaches for selection and ensembling of GCMs. *Journal of Water and Climate Change* **11**, 577–599. https://doi.org/10.2166/wcc.2020.128.

Sadhwani, K., Eldho, T. I. & Karmakar, S. 2023 Investigating the influence of future landuse and climate change on hydrological regime of a humid tropical river basin. *Environmental Earth Sciences* **82**, 1–19. https://doi.org/10.1007/s12665-023-10891-6.

Shaaban, A. J., Amin, M. Z. M., Chen, Z. Q. & Ohara, N. 2011 Regional modeling of climate change impact on Peninsular Malaysia water resources. *Journal of Hydrologic Engineering* **16**, 1040–1049. https://doi.org/10.1061/(asce)he.1943-5584.0000305.

Sharma, A., Patel, P. L. & Sharma, P. J. 2022 Influence of climate and land-use changes on the sensitivity of SWAT model parameters and water availability in a semi-arid river basin. *Catena* **215**, 106298. https://doi.org/10.1016/j.catena.2022.106298.

Singh, J., Knapp, H. V., Arnold, J. G. & Demissie, M. 2005 Hydrological modeling of the Iroquois River watershed using HSPF and SWAT. *Journal of the American Water Resources Association* **41**, 343–360. https://doi.org/10.1111/j.1752-1688.2005.tb03740.x.

Srivastava, A. K., Rajeevan, M. & Kshirsagar, S. R. 2009 Development of a high resolution daily gridded temperature data set (1969–2005) for the Indian region. *Atmospheric Science Letters* **10**, 249–254. https://doi.org/10.1002/asl.

Sudheer, K. P., Murty Bhallamudi, S., Narasimhan, B., Thomas, J., Bindhu, V. M., Vema, V. & Kurian, C. 2019 Role of dams on the floods of August 2018 in Periyar River Basin, Kerala. *Current Science* **116**, 780–794. https://doi.org/10.18520/cs/v116/i5/780-794.

US Army Corps of Engineers. 2018 *Hydrologic Modeling System HEC-HMS, User's Manual*. Hydrologic Engineering Centre, Davis, CA.

Wijayarathne, D. B. & Coulibaly, P. 2020 Identification of hydrological models for operational flood forecasting in St. John's, Newfoundland, Canada. *Journal of Hydrology: Regional Studies* **27**, 100646. https://doi.org/10.1016/j.ejrh.2019.100646.

Yaduvanshi, A., Sharma, R. K., Kar, S. C. & Sinha, A. K. 2018 Rainfall–runoff simulations of extreme monsoon rainfall events in a tropical river basin of India. *Natural Hazards* **90**, 843–861. https://doi.org/10.1007/s11069-017-3075-0.

Zhang, A., Liu, W., Yin, Z., Fu, G. & Zheng, C. 2016 How will climate change affect the water availability in the Heihe River Basin, Northwest China? *Journal of Hydrometeorology* **17**, 1517–1542. https://doi.org/10.1175/JHM-D-15-0058.1.

First received 15 November 2022; accepted in revised form 4 June 2023. Available online 14 June 2023